Empowering Antibiotic Polymer Design through Coarse-Grained Molecular Dynamics

Gabriel N. Serafim,[*,†] Manuel N. Melo,[*,‡] Vasco D. B. Bonifácio,[*,†] Sandra N. Pinto,[*,†] and Nuno Martinho[*,†]

†*Institute for Bioengineering and Biosciences, Instituto Superior Técnico, Universidade de Lisboa, Lisbon*

‡*Instituto de Tecnologia Química e Biológica, Universidade Nova de Lisboa, Oeiras*

E-mail: gabriel.serafim@tecnico.ulisboa.pt; m.n.melo@itqb.unl.pt; vasco.bonifacio@tecnico.ulisboa.pt; sandrapinto@tecnico.ulisboa.pt; nunomartinho@tecnico.ulisboa.pt

Abstract

Antibiotic resistance traits appear when bacteria are still able to grow in the presence of therapeutic concentrations of antibiotic drugs. As an alternative for the current antibiotics crisis, the development of bio-mimetic polymers is a field with great potential. In this work, a coarse-grained Martini model of a therapeutic nanoparticle and proposed modifications were built and tested against models of phospholipid bilayer membranes to understand what are the possible mechanisms that provide their antimicrobial activity and selectivity. The results showed that positive net charge is crucial to display the desired selectivity, causing negative curvatures that may induce further permeabilization and/or disruption. Leucine modification increased the hydrophobic content and improved the distance between the nanoparticle and the center of the membrane, without losing the desired selectivity. Furthermore, the nanoparticle's ability to alter the ionic distribution in the membrane environment can be an indicative of a different mode of action.

1 Introduction

For decades, multiple varieties of antibiotics have not only been used for therapeutic purposes but also as prophylactic practice across industries such as agriculture and animal husbandry. In the past decades the production of new classes of antibiotics has increased exponentially due to the demand across many sectors and allowed for less expensive and off-label drugs. As a side effect, the wide availability of different compounds that possess antimicrobial properties and increased irresponsible use of these drugs have contributed significantly to the advent of resistant strains of microbes and the reduction of their capability to fight infections caused by those microorganisms.[1]

The consequence of antibiotic resistance has already shown its impacts around the world. The World Economic Forum has identified antibiotic resistance as a global risk beyond the capacity of any organization or nation to manage or mitigate alone.[2] The Europe Union has reported that, annually, around 25000 deaths are due to a subset of drug resistant bacteria, with the extra health care costs and lost productivity due to antimicrobial resistance amounting to at least 1500€ million. Similar impacts should also be present in low- and middle-income countries.[3]

From the rising challenge of fighting the insurgence of antimicrobial resistant microbes, it became necessary to develop new alternatives different from the traditional antibiotics used

until current days.[4] In the early 2000s, the fields of host defense peptides (HDPs) and biocidal polymers started to merge seeking the development of HDP-mimetic polymers. The rationale behind this merge is to combine the advantages of peptide activity with the cost effectiveness and scalability of synthetic polymer chemistry, without the need for precise sequence, unimolecular chain length, or defined secondary structure.[5] Although HDPs are excellent potential substitutes for antibiotics, due to their antimicrobial and non-toxic characteristics, the bioprocesses involved in the manufacture of cheap and scalable volumes are still not developed enough.[6] At the same time, while chemical processes are well known and developed enough for production in large scale, the potential toxicity of these compounds is something that cannot be neglected.[6]

By having the possibility to change and tune synthetic polymers to present the desired functionality, a huge variety of options can be manufactured. The rise of high-performance computing has enabled experimentation *in silico* as a powerful tool that bridges the gap between theory and laboratory experiments.[7] Taking into consideration that bio-mimetic antimicrobial polymers demonstrate to have some type of interaction with microbial membranes, it is important to have a tool that predicts whether the molecule being tested has promising interactions and effects. In this sense, Molecular Dynamics (MD) can be an important computational tool for understanding the physical basis of structure, dynamic evolution of systems, and the function of biological macro-molecules[8] and to directly aid in the development of new drugs.

This work main goal is to apply computational tools to power the development of bio-mimetic antimicrobial nanoparticles. This was done by exploring and trying to gain insight on the killing mechanism of an already existing nanoparticle by means of MD simulations. The studied nanoparticle - $PURE_{G4}$-OEI_{48} - is a fourth-generation polyurea dendrimer ($PURE_{G4}$) core with 48 linear oligo(ethylenimine) chains (OEI_{48}) connected to its surface. For this it was necessary to develop and build the corresponding coarse-grained (CG) model of the nanoparticle being investigated and run simulations against CG membrane models that can capture the difference between bacterial (POPC/POPG - 1:3 ratio) and mammalian (POPC) phospholipid bilayers. The results from these simulations enable the proposal of modifications to synthesize novel nanoparticles with the enhanced functionality and biophysical properties.

2 Methodology

2.1 All-atom Molecular Dynamics

To perform all MD simulations, Gromacs version 2018.3[9] or higher were used implementing a leap-frog algorithm for integrating Newton's equations of motion with a time step of 2 fs. The neighbor searching as set with Verlet cut-off scheme with grid type and a cut-off distance of 14 Åfor both Van der Waals and Coulombic interactions. Periodic boundary conditions were applied in all directions, while the system was solvated with TIP3P water model and the long-range electrostatic interactions were treated with the Particle Mesh Ewald (PME) method of order 4 and using a grid spacing of 1.6 Å. The temperature was fixed at 300 K using a temperature coupling using velocity rescaling with a stochastic term with time constant of 1 ps. Pressure has treated using Parrinello-Rahman coupling with isotropic type, time constant of 5 ps and reference pressure of 1 bar.

2.2 Coarse-grained Molecular Dynamics

All CG MD simulations were carried out using Gromacs version 2018.3 or higher employing leap-frog propagation with a time step of 20 fs, a Verlet cut-off scheme of type grid and periodic boundary conditions in all directions using a 11 Åcutoff for the short-range interactions (Van der Waals and Coulombic interactions). Long range electrostatics were treated with the reaction field method with a relative dielectric constant $\epsilon_r = 15$ in conjunction with with standard water beads, and infinite screening beyond the cutoff distance. The temperature was kept fixed at 300 K using stochastic velocity rescaling with a (weak) coupling constant of 1 ps, while pressure has treated using Parrinello-Rahman coupling with isotropic type, time constant of 12 ps and reference pressure of 1 bar.

The membrane systems were minimized and equilibrated as the $PURE_{G4}$-OEI_{48} nanoparticle, with the difference that

semi-isotropic pressure coupling was used, to decouple solvent pressure in z from membrane tension in xy. Both minimization an equilibration were performed with a restraint at the central bead of the nanoparticle to avoid displacement towards the membrane during these steps. All production simulations were run for at least 3 μs.

2.3 End-to-end distance, D_{ee}

The end-to-end distance, D_{ee} correspond to the norm of the vector that points from one end of the polymer chain to the other. This property helps indicate how extended a polymer chain is.

2.4 Radius of Gyration, R_g

The Radius of Gyration (R_g) was used to determine if the topology generated could reproduce the same behavior as the one measured from the atomistic model. R_g corresponds to the root mean square of distance from all beads to the particle center of mass.

2.5 Shape Parameter, S and Asphericity, Δ

To evaluate the general shape that the particle assumes along the entire trajectory, two properties were investigated: the shape parameter (S), that evaluates the shape itself, and asphericity (Δ) that is an indication of the extent of the shape's anisotropy. [10]

S can assume values from (-1/4) up to 2. The negatives values indicate an oblate shape, whereas positive values indicate a prolate shape; a perfect sphere yields $S = 0$.In the same fashion as S, Δ will take values from 0 up to 1, where zero indicates the perfect isotropy of a sphere, and 1 maximal anisotropy.

2.6 Radial distribution function, $g(r)$

The radial distribution function ($g(r)$ or RDF) describes how the density of a certain system component, relative to the bulk, varies as a function of the distance to a reference. An interparticle RDF is calculated by histogramming the distances between all particles pairs from a test and a reference groups, a and b.

This equation is normalized to the bulk density of the test group, so that for large distances in a macroscopically homogeneous system the RDF tends to 1 (indicating no influence from one particle on another's position at large distances).

2.7 Distance-to-core

The distance to the core of the membrane was defined as the minimum distance between each external bead of the nanoparticle's dendrimer layer (the beads that anchor the polymer chains) and the last beads of the phospholipids tails (C4A and C4B) of each membrane's inner leaflet. This metric is being used as a proxy for particle–membrane in-depth interaction but without the requirement that a membrane normal be defined — which can be troublesome where there is membrane curvature. Results were expressed in the form of histograms.

3 Results and discussion

3.1 Poly(ethylenimine) Martini 3 Model

The modeling of our Martini 3 PEI starts out by defining the CG beads mapped to represent the residues defined in the Amber model (terminal residues, encompassing 1.5 units each, are represented by two beads). Figure 1 shows the mapping used for all PEI chains, where both three-to-one (S or 'small', green) and two-to-one (T or 'tiny', blue) bead types are used. The beads' respective mass-centers and identifications are: 1) TBP: terminal protonated bead - $NH_3^+{-}CH_2$ - 2) TBN: terminal non-protonated bead - $NH_2{-}CH_2$ - 3) MBP: protonated monomer bead - $CH_2{-}NH_2^+{-}CH_2$ - 4) MBN: non-protonated monomer bead - $CH_2{-}NH{-}CH_2$.

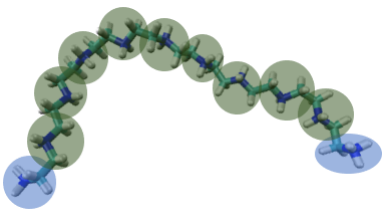

Figure 1: Mapping scheme for fully-protonated PEI chains. Blue bead represents TBP (or TBN for non-protonated chains) and green represents MBP (or MBN for non-protonated and semi-protonated chains).

Beads without charge were assigned the type N, since they

represent moderately-to-weakly polar groups; of those, beads encompassing NH_2 will receive a hydrogen-bond-donor label (d), since they have one more hydrogen bond donor than acceptors, while beads with NH are going to be regular (no such label), since they have the same number of hydrogen-bond donors and acceptors. To determine the size of the beads, an S or T prefix indicates small and tiny beads, respectively, while normal size (four-to-one mapping) beads have no prefix. Finally, the polarity level within each type is dictated by the production of partition behavior, leading to the following assignment: 1) TBP: $NH_3^+-CH_2$ - TQ4p - 2) TBN: NH_2-CH_2 - TN6d - 3) MBP: $CH_2-NH_2^+-CH_2$ - SQ3p - 4) MBN: $CH_2-NH-CH_2$ - SN3.

All bonds, bending angles and dihedral angles parameters were successfully obtained after performing sequels trial and error simulations runs. The validation of these parameters was done by comparing emergent properties of the PEI, such as the average simulated D_{ee} and R_g, that should match between atomistic and CG simulations. Comparison with the literature also also made. Figure 2 depicts the averaged end-to-end distance and radius of gyration for the no salt condition for the CG simulations (marked as void circles) and the reference AA values (marked as full circles).

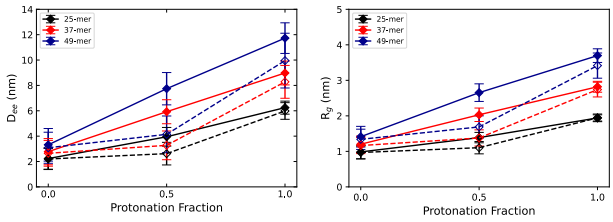

Figure 2: End-to-end distance and radius of gyration for PEI chains under no salt condition. AA values are represented by full circles and continuous lines while CG are void circles with dashed lines.

Both plots at Figure 2 show that the CG model developed can reproduce the atomistic behavior of the non- and fully-protonated states of the linear PEI. Another observation is that there may be a small tendency for the values from the CG simulations to be lower than the ones from AA. This is partly explained by the fact that parameterization was performed emphasizing the reproduction of behavior at high ionic strengths, where the polymer is less extended. Nevertheless, the values are still within the error of each other.

For the semi-protonated, we can observe that the CG model under-represents the behavior of the polymer when semi-protonated, with the values of R_g and D_{ee} being, on average, 29 and 41% smaller then the atomistic one. The excessive compactness of the CG model for this protonation state is a consequence of the coarseness with which explicit charges are treated in Martini: because water is not explicitly polar (polar/polarizable CG water models do exist [11] but are not yet developed for Martini 3) dielectric screening is mimicked by a large relative permittivity of 15 in the simulation. This implicit screening seems to overly dampen electrostatic interactions at the longer distances involved in nonconsecutive amine repulsion. The same shortcomings were observed by Beu et al. for Martini 2, where a correction could be made by using a polarizable water model [11] — at the cost of a heavier computational effort.

When looking into the simulations under salt conditions (fig. 3), we are able to see that the agreement between CG and AA models for the the semi-protonated state improves by about 40% for both the averaged D_{ee} and R_g. This, again, can be explained by the excess of positively and negatively charges provident of NaCl that explicitly mediate the electrostatic interactions within the system, and thus also explaining a better agreement for the non and fully protonated versions.

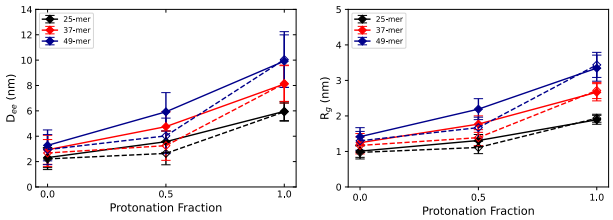

Figure 3: End-to-end distance and radius of gyration for PEI chains under 150mM of NaCl. AA values are represented by full circles and continuous lines while CG are void circles with dashed lines.

3.2 Polyurea Martini 3 Model

The Martini 3 representation of the polyurea is centered at two well defined chemical groups: the urea and the tertiary amine. The most suitable mapping consisted in a larger representation where certain CH_2 groups were shared between

beads. This strategy led to a five-to-one representation for the beads centered on the urea groups and a "five-and-a-half"-to-one for the beads centered on the tertiary amines, with each shared methylene (CH_2) counting as half towards each bead. Figure 4 shows the representation of the tertiary amine (AM) and urea (UR) centered beads for the coarse-grained topology:

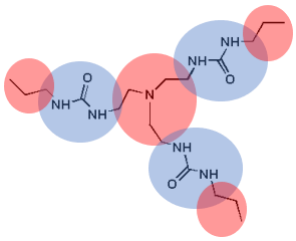

Figure 4: AM (amine; red) and UR (urea; blue) beads that represent the general mapping choice for the $PURE_{G4}$ dendrimer. Three extra red circles represent the amine groups of the dendrimer's next generation.

All beads were treated as regular size beads. The AM bead, defined by a triethylamine scaffold, is considered to be nonpolar (type N) and receives an *a* label that represents the capacity to accept hydrogen bonds, while the UR bead, with its dimethylurea frame, is a polar (P) type bead, also with capacity to accept hydrogen bond and having the same *a* label. The choice of interaction level was slightly tuned down from its reference and the level 3 and 4 were assigned, respectively, for AM and UR beads. To finish the bead type assignment all terminal NH_3^+ will be treated as TQ4p and named as 'NT' beads. This matches what was used as the first bead of the OEI chain topology.

All bonds and bending angles parameters were successfully obtained after performing sequels trial and error simulations runs. The validation of these parameters was done by comparing emergent properties of the dendrimer, such as the average simulated R_g, that should match between atomistic and CG simulations. Table 1 shows that the CG is quite able to reproduce the physiochemical property of interest. The table hints that the CG topology may have a small deviation into a prolate shape and some asymmetry compared to the atomistic behavior, but not significantly enough to negate its validity.

Table 1: Average Radius of gyration, Shape parameters and Asphericity comparison between Atomistic and Coarse-grained topologies for $PURE_{G4}$. All values are in Å.

	Atomistic	Coarse-grained
$\langle R_g \rangle$	21.44 ± 0.43	21.08 ± 1.09
$\langle \mathbf{S} \rangle$	0.001 ± 0.013	0.025 ± 0.045
$\langle \Delta \rangle$	0.050 ± 0.014	0.090 ± 0.045

3.3 Nanoparticle's structure

Having built the Martini 3 topology for $PURE_{G4}$-OEI_{48} nanoparticle, it is imperative to check and understand its dynamics. To better understand the dynamics characteristics studied, all parameters were calculated considering two distinct groups of beads. First group consist solely of the beads of the dendrimer layer while the second one corresponds to the whole nanoparticle. Since the dynamics of the dendrimer was already studied separately, this strategy helps to point the contribution of the polymers' chains and, consequently, its protonation (Table 2).

Table 2: Average Radius of gyration (in Å), Shape parameters and Asphericity of all three state of protonation from $PURE_{G4}$-OEI_{48}.

	Fully-protonated		Half-protonated		Non-protonated	
	Dendrimer	Nanoparticle	Dendrimer	Nanoparticle	Dendrimer	Nanoparticle
$\langle R_g \rangle$	19.723 ± 0.622	30.338 ± 0.894	20.889 ± 0.530	29.524 ± 0.638	19.562 ± 0.805	26.043 ± 1.034
$\langle \mathbf{S} \rangle$	0.022 ± 0.031	0.006 ± 0.014	-0.004 ± 0.018	0.000 ± 0.007	0.008 ± 0.040	0.006 ± 0.022
$\langle \Delta \rangle$	0.094 ± 0.039	0.039 ± 0.024	0.054 ± 0.025	0.026 ± 0.014	0.085 ± 0.041	0.053 ± 0.029

From the table above its possible to notice that the average R_g for the dendrimer layers has the same value (considering the error) across all three-protonation situation. That shows that the polymer chains that are attached has close to no effect in the dynamics of the dendrimer itself. When considering the whole particle, the difference in the average values of R_g starts to get the expected contribution from the polymer's behavior in solution, as the size if the nanoparticle increases with the degree of protonation.

The shape assumed by $PURE_{G4}$-OEI_{48} is almost perfectly spherical, since the average S is close to zero, independent of the state. The slightly anisotropy observed can be attributed to the minute deviation to a prolate shape, that is mostly being a contribution of the dendrimer.

3.4 Nanoparticle at membrane environment

Both fully and half-protonated states were able to create binding pocket by forming negative curvatures after their in-

teractions with the POPC/POPG system. It was possible to observe two different type of curvatures interaction that can lead to some form of mechanism behind the antimicrobial activity of PURE$_{G4}$-OEI$_{48}$ (Fig. 5).

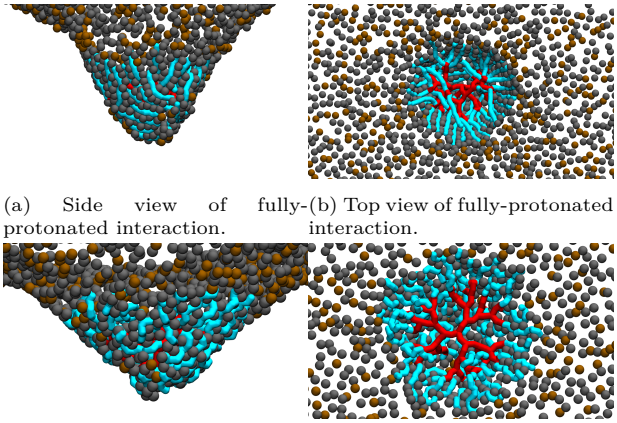

(a) Side view of fully-protonated interaction.

(b) Top view of fully-protonated interaction.

(c) Side view of half-protonated interaction.

(d) Top view of fully-protonated interaction.

Figure 5: Side and top view of PURE$_{G4}$-OEI$_{48}$ interaction with POPC/POPG membrane, where red represents the dendrimer core, blue the OEI chains, gray the PO_4^- beads from POPG and brown PO_4^- from POPC.

In the case of the fully-protonated state, this cavity is deeper, and the OEI chains are arranged in an alternating and radial manner between the PO_4^- (dark gray beads) from POPG. For the half-protonated, the cavity generated had less depth and the organization of the polymer chains along the PO_4^- does not seem to follow a distinguished pattern. This behavior can be explained by the difference in positive charge density express by each protonation state.

The ability to induce curvatures has also been identified as one of the ways of HDPs to compromise the barrier function of membranes.[13] Negative curvatures display the capacity to sort and modify the arrangement of cardiolipin (CL) into clusters[14] and bacterial cell membranes contain greater amounts of both anionic and negative intrinsic curvature lipids (such as CL) are more susceptible to be destabilized by deformation from curvatures.[13] Curvatures (either negative or positive) increase the permeability to hydrophilic compounds.[15]

The distance-to-core analyze helps get a better insight regarding the difference interaction between protonation states. From these plot (Fig.6) we can first observe a higher selectivity towards charged states.The absence of positive charge results in the nanoparticle interacting with both membrane types in a similar manner.

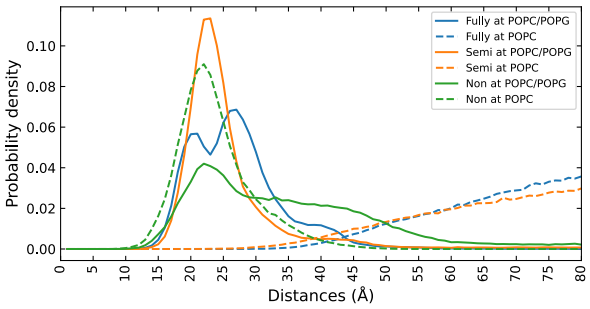

Figure 6: Distance-to-core distribution for PURE$_{G4}$-OEI$_{48}$ and POPC/POPG (solid) or POPC (dashed) membranes, at the three protonation levels.

Ions are essential to the correct metabolic function of all organism as they take part as being cofactors for enzymes, are involved into redox reactions and energetic pathways and also are crucial for the maintenance of the osmotic pressure of cells. Any limitation or imbalance of those micronutrients can drive delay in cell growth or even cause cell death.[16]

To understand the way that the ions of the system (Na^+ and Cl^-) are distributed at the proximity of the outer leaflet of both POPC/POPG and POPC membranes, their radial distribution function relative to the membrane was used and the results for the fully-protonated nanoparticle are shown in Fig. 7. This analysis was performed considering two distinct groups for each of the ions involved, divided into "close" and "far" groups, according to whether they are PO_4^- within 3 nm of the nanoparticle ("close") or not ("far"). From Figure 7 it is possible to notice that the Na^+ distribution changes a lot at the regions where the nanoparticle interacts with the membrane. The presence of this cation is reduced by around 3-fold in the vicinity of the membrane regions interacting with a nanoparticle, when compared to the regions that do not. The plot also shows that the Cl^- ions are dragged by the nanoparticle and their concentration increases at closer distances to the membrane when it interacts with the nanoparticle. In contrast to the ionic distribution around POPC/POPG membranes, Figure 7 shows that Na^+ concentration stays uniform along the whole extension of the POPC membrane, even when nanoparticle contacts do occur (both orange lines completely superimpose). The nanoparticle does not interact with non-ionic

phospholipids, neither does it disturb their ionic shells.

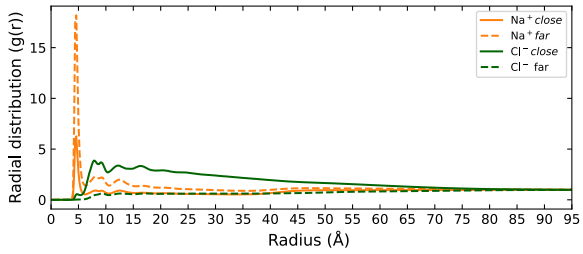

(a) Original nanoparticle at POPC/POPG

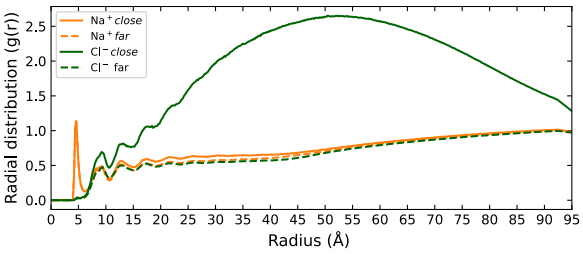

(b) Original nanoparticle at POPC

Figure 7: Radial distribution function of ions around outer leaflet of membranes under presence of fully-protonated PURE$_{G4}$-OEI$_{48}$. Note that in b) the Na^+ plots completely superimpose at distances below 7 Å, as do the plots for Cl^-.

With the property to interact with different types of anions, it is possible that one mode of action related to the antimicrobial ability of PURE$_{G4}$-OEI$_{48}$ is to form a layer around the bacterial cell that will alter the concentration distribution of cations and anions and progressively disrupt ion-dependent functions, leading to cell death.

3.5 Modifications

With the knowledge acquired, the next step was to study possible modifications to the original PURE$_{G4}$-OEI$_{48}$ that may increase its overall antimicrobial effects. The objective was to increase the hydrophobic interaction of the whole nanoparticle with the membrane by taking advantage of already known parameterized building block in Martini 3. Following this strategy, amino acid residues were suitable starting points for the development of modifications of the original nanoparticle. For this study, Leucine (leu), Phenylalanine (phe) and Tryptophan (trp) were chosen for their side-chain hydrophobicity (from the Wimley–White whole residue hydrophobicity scales[17,18]), and their different propensities for interfacial membrane interaction. A total of 48 amino acids residues were inserted between the dendrimer and the polymer chains, one per dendrimer–polymer link, forming a lipophilic layer. The bonds and angles parameters between AM beads from the dendrimer, the BB beads from amino acids residues and NT beads from OEI chains were drawn directly from the Martini 3 parameters for a random-coiled protein backbone.

Prior to analyzing whether any of the suggested modifications improve the nanoparticle's antimicrobial activity, we check dynamic behavior to understand if the alterations cause any significant changes.In regard to the size, it was possible to notice that the phenylalanine and tryptophan modifications reduce the average values for both the dendrimer layer and for the whole particle at all protonation states. This may be explained by the relative size and presence of aromatic ring of those residues, which favors the occurrence of π stacking interactions and a small collapse of this lipophilic layer, countering the expansion of the nanoparticle as a whole.

In terms of shape and asphericity, again, the phenylalanine and tryptophan residues have more impact than leucine. Both increased the deviation of the shape to a more prolate configuration and increase its asphericity. However, the effect of polymer chain protonation still dominates, and amino acid contribution becomes more visible for non-protonated chains. In general, however, amino acid effects are small, probably because the nanoparticle can undergo large changes at its core without major implications at the overall size and shape.

The fully-protonated plot (Fig. 8), shows that while all modifications have a similar interaction with POPC/POPG membranes as the original nanoparticle, their distributions reach significantly lower distances, meaning that they can get closer to the center of the membrane. Interestingly, while leucine and tryptophan modifications do not significantly come to contact with the POPC membrane, the phenylalanine modification is able to interact with it (green dashed curve), going against what is expected for positively charge particles and its lack of selectivity toward neutral membranes. As an explanation to this action, it is possible that the hydrophobic character brought by the insertion of 48 phenylalanine residues can counter the effects of the charge and allows for the contact observed; its size and high hydrophobicity compared to the other

two amino acids can also be factors behind this observation.

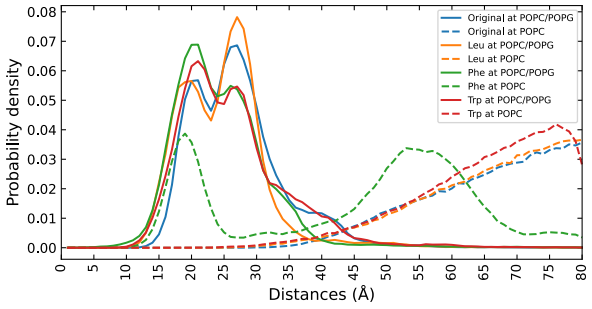

Figure 8: Distances probability of fully-protonated nanoparticles at POPC/POPG (solid) and POPC(dashed) membranes.

When analyzing the half-protonated state (fig. 9), membrane penetration is likewise increased relative to the original nanoparticle.

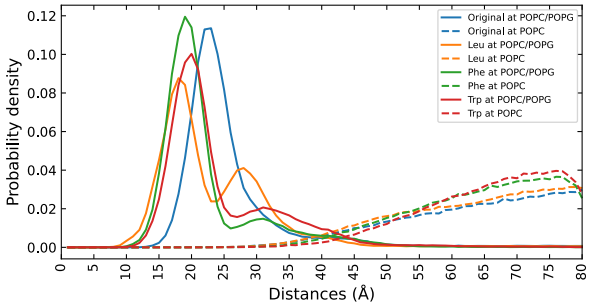

Figure 9: Distances probability of half-protonated nanoparticles at POPC/POPG (solid) and POPC (dashed) membranes.

The visual inspection of the relevant trajectories come as another source of evidence from the analysis made so far. First, the mode of action for the fully-protonated phenylalanine modification among the two types of membrane can be observed in figure 10:

The overall charge density resulting from all polymer chains makes the interaction with POPC/POPG membrane to be quite similar to the one from the original nanoparticle. In this situation, it's possible to see that the amino acid moieties can pass between PO_4^- heads and better interact with the phospholipids' hydrophobic interface/tail region (Fig. 10a). This interaction may help to approximate the whole nanoparticle to the center of the bilayer and increase the tension of the cavity formed. In the scenario with the POPC membrane, the interaction is mainly ruled by the amino acids' residues. This visualization confirms that there is an equilibrium between the

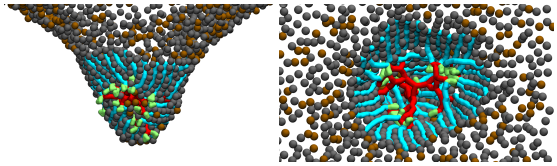

(a) Side view of interaction with POPC/POPG.

(b) Top view of interaction with POPC/POPG.

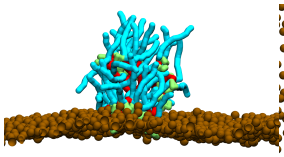

(c) Side view of interaction with POPC.

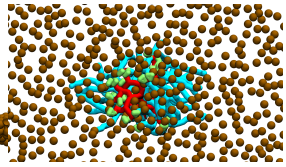

(d) Bottom view of interaction with POPC.

Figure 10: Trajectory views of fully-protonated Phenylalanine mod PURE$_{G4}$-OEI$_{48}$ interaction with POPC/POPG and POPC membranes.

repulsion from the positives charges of the nanoparticle and the lipophilic affinity from amino acids. When the nanoparticle is able to get to a certain distance from the outer leaflet and expose the amino acids, it becomes anchored through the affinity of phenylalanine for the phospholipids (Fig. 10c and 10d). The prolate shape of the phenylalanine-modified nanoparticle leads to two possible interaction orientations (the upright stance seen in Fig. 10b and a horizontal one), explaining the two distance peaks in figure 8.

The interactions of the other two modifications, in the fully-protonated state, are presented in Figure 11. Both side views (Fig. 11a and 11c) show similar cavity formation as seen so far, although this effect is not as prominent for the tryptophan modification.

In contrast with the protonated state, the half-protonated interaction of all modifications (Fig. 12) has significant deviations from the original one in that the formed cavity is not as deep. Here, cavity formation competes with a broader nanoparticle–membrane interaction due to increased amino acid solubility into the lipid tails, which does not become completed due to the anchoring of the positive charges at the membrane surface. From the interaction of the leucine modification (Fig. 12a) one can see that some parts of the dendrimer layer are able to pass the phosphate barrier. The same happens for the other two modifications, but to a lesser extent. From all the top views (fig. 12b, 12d and 12f) the number of residues that can interact at the same time with the membrane seems to

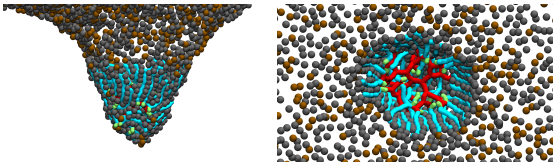

(a) Leucine mod side view interaction

(b) Leucine mod top view interaction

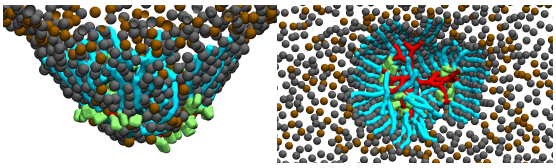

(c) Tryptophan mod side view interaction.

(d) Tryptophan mod top view interaction.

Figure 11: Trajectory views of fully-protonated Leucine and Tryptophan mods $PURE_{G4}$-OEI_{48} interaction with POPC/POPG membranes.

be higher than in the previous state. This higher contribution of lipophilic groups seems to increase the proximity and may allow for stronger/different mechanisms of disruption.

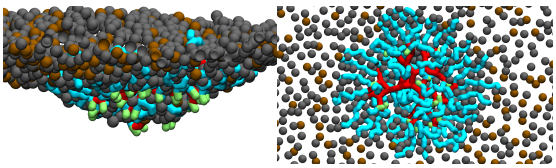

(a) Leucine mod side view interaction

(b) Leucine mod top view interaction

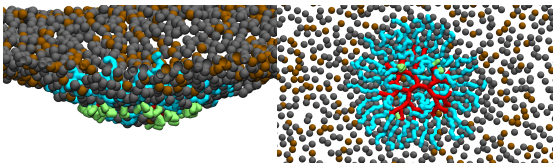

(c) Phenylalanine mod side view interaction.

(d) Phenylalanine mod top view interaction.

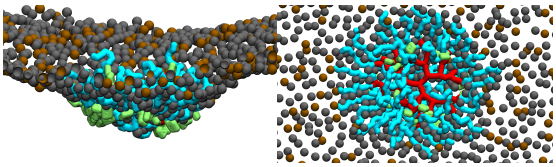

(e) Tryptophan mod side view interaction.

(f) Tryptophan mod top view interaction.

Figure 12: Trajectory views of half-protonated mods $PURE_{G4}$-OEI_{48} interaction with POPC/POPG membranes.

The possible impact of the addition of amino acids on the ionic distribution of the system were investigated. All results demonstrate that the addition of the modifications has practically no influence at how ions distribute. For all the simulated scenarios, the protonation state still dictates the interaction with ions, closely following the same pattern displayed by the the original nanoparticle.

4 Conclusions

The desire to better understand how therapeutic nanoparticles, designed from the principles behind the antimicrobial activity of AMPs, act against bacteria drove the development of this study and the use Molecular Dynamics as a powerful tool in the design of novel antibiotics molecules.

The ability to perform large scale studies, either in time and/or system size, favors the choice of a coarse-grained approach instead of an all-atom one. The Martini force field, being the most popular CG model to date and having a precise behavior in regard to lipid interaction becomes the most suitable choice. With the upcoming release of an updated version of this FF, Martini 3 has the potential to provide more refined and accurate models without the loss of its intrinsic low simulation cost.

The whole parameterization process expanded for the linear poly(ethylenimine) shows the importance of having a solid theoretical background to support the model created. The ability to investigate how this specific polymer chain behaves in different scenarios, mainly those that approach the conditions of their potential applications, helps demonstrate the strength of using MD simulations to screen multiple options and conditions prior laborious or costly experimental work is done. Here we were able to observe how different protonation states and the presence of ionic strength can impact the polymer's structural dynamics — including those of the linear OEI chain, of the polyurea dendrimer and of the assembled nanoparticle models. The nanoparticles were then simulated to infer how they interact with, and potentially disrupt, model membranes. These computational findings, including the proposal of increased activity modifications, lay the foundation for future experimental studies which can not only complement and validate our work by hopefully producing more potential therapeutic nanoparticles, but can also help in creating more refined and realistic molecular models.

The analysis made in this project contributed to the overall understanding of how custom designed nanoparticles inter-

act with distinct types of membrane models. For a therapeutic nanoparticle to have an optimal antimicrobial effect, it requires a tight balance between the density of its overall positive charge and the extent of its hydrophobic groups. The results show that the positive net charge is crucial in dictating selectivity, allowing for the interaction with anionic phospholipids but, without a significant amount of hydrophobic interaction, the nanoparticle can't break the electrostatic barrier imposed by the membrane and diffuse into or disrupt the phospholipid bilayer. This work was able to improve the balance between charge and hydrophobicity by the insertion of leucine amino acids which results in improved interaction than the ones from the original nanoparticle.

In all, the work developed here is an important first step in search for insight into the killing mechanism of these types of nanoparticles. Further theoretical works can expand from this starting point, where new modifications (*e.g.* insertion of hydrophobic moieties at different regions of the polymer or dendrimer structure) and more robust bacterial membrane models can be tested and lead the design of polymeric nanoparticles. Likewise, as previously mentioned, future experimental studies can utilize this work as a guide, which can facilitate and assist at the production of more safe and effective therapeutic nanoparticles.

Acknowledgement

This document was written and made publically available as an institutional academic requirement and as a part of the evaluation of the MSc thesis in Bioengineering and Nanosystems of the author at Instituto Superior Técnico. The work presented in this thesis was performed at the Multiscale Modeling Lab at Instituto de Tecnologia Química e Biológica António Xavier from Universidade Nova de Lisboa (Oeiras, Portugal), during the period of August/2019 to October/2020, under the supervision of Dr. Manuel Nuno de Sousa Pereira Simões de Melo. The thesis was co-supervised in the BSIRG group at Institute for Bioengineering and Bioscience from Instituto Superior Técnico (Lisbon, Portugal) by Dr. Vasco Daniel Bigas Bonifácio, Dr. Nuno Martinho and Dr. Sandra Pinto.

References

(1) Tacconelli, E.; Carrara, E.; Savoldi, A.; Kattula, D.; Burkert, F. *GLOBAL PRIORITY LIST OF ANTIBIOTIC-RESISTANT BACTERIA TO GUIDE RESEARCH, DISCOVERY, AND DEVELOPMENT OF NEW ANTIBIOTICS*; 2017.

(2) World Economic Forum, *Global Risks 2013 Eighth Edition An Initiative of the Risk Response Network Insight Report*; 2013.

(3) World Health Organization, *Global Action Plan on Antimicrobial Resistance*; 2015.

(4) Gibney, K. A.; Sovadinova, I.; Lopez, A. I.; Urban, M.; Ridgway, Z.; Caputo, G. A.; Kuroda, K. Poly(ethylene imine)s as antimicrobial agents with selective activity. *Macromolecular Bioscience* **2012**, *12*, 1279–1289.

(5) Ergene, C.; Yasuhara, K.; Palermo, E. F. Biomimetic antimicrobial polymers: Recent advances in molecular design. 2018.

(6) Wang, G.; Li, X.; Wang, Z. APD3: The antimicrobial peptide database as a tool for research and education. *Nucleic Acids Research* **2016**, *44*, D1087–D1093.

(7) Aminpour, M.; Montemagno, C.; Tuszynski, J. A. An Overview of Molecular Modeling for Drug Discovery with Specific Illustrative Examples of Applications. *Molecules* **2019**, *24*, 1693.

(8) Karplus, M.; McCammon, J. A. Molecular dynamics simulations of biomolecules. 2002.

(9) Abraham, M.; van der Spoel, D.; Lindahl, E.; Hess, B.; development team, G. GROMACS User Manual version 2018. *GROMACS User Manual* **2018**,

(10) Dima, R. I.; Thirumalai, D. Asymmetry in the shapes of folded and denatured states of proteins. *Journal of Physical Chemistry B* **2004**, *108*, 6564–6570.

(11) Yesylevskyy, S. O.; Schäfer, L. V.; Sengupta, D.; Marrink, S. J. Polarizable water model for the coarse-grained MARTINI force field. *PLoS Computational Biology* **2010**, *6*, 1–17.

(12) Beu, T. A.; Ailenei, A.; Costinaş, R. Martini Force Field for Protonated Polyethyleneimine. *Journal of Computational Chemistry* **2020**, *41*, 349–361.

(13) Schmidt, N. W.; Wong, G. C. Antimicrobial peptides and induced membrane curvature: Geometry, coordination chemistry, and molecular engineering. 2013.

(14) Beltrán-Heredia, E.; Tsai, F. C.; Salinas-Almaguer, S.; Cao, F. J.; Bassereau, P.; Monroy, F. Membrane curvature induces cardiolipin sorting. *Communications Biology* **2019**, *2*.

(15) Yesylevskyy, S.; Rivel, T.; Ramseyer, C. Curvature increases permeability of the plasma membrane for ions, water and the anti-cancer drugs cisplatin and gemcitabine. *Scientific Reports* **2019**, *9*.

(16) van Vliet, A. H. M.; Bereswill, S.; Kusters, J. G. *Helicobacter pylori*; ASM Press, 2014; pp 193–206.

(17) White, S. H.; Wimley, W. C. Hydrophobic interactions of peptides with membrane interfaces. 1998.

(18) White, S. H.; Wimley, W. C. Membrane protein folding and stability: Physical principles. *Annual Review of Biophysics and Biomolecular Structure* **1999**, *28*, 319–365.